**Article:**
Alosaimi, M, Lesnic, D orcid.org/0000-0003-3025-2770 and Niesen, J orcid.org/0000-0002-6693-3810 (2020) Reconstruction of the thermal properties in a wave-type model of bio-heat transfer. International Journal of Numerical Methods for Heat & Fluid Flow. ISSN 0961-5539

https://doi.org/10.1108/HFF-10-2019-0776

# Reconstruction of the thermal properties in a wave-type model of bio-heat transfer

Moataz Alosaimi[1,2], Daniel Lesnic[1] and Jitse Niesen[1]

[1]Department of Applied Mathematics, University of Leeds, Leeds LS2 9JT, UK
[2]Department of Mathematics, Taif University, Taif P.O. Box 888, Saudi Arabia
E-mails: mmmaal@leeds.ac.uk (M. Alosaimi), amt5ld@maths.leeds.ac.uk (D. Lesnic), j.niesen@leeds.ac.uk (J. Niesen)

E-mails: mmmaal@leeds.ac.uk (M. Alosaimi), amt5ld@maths.leeds.ac.uk (D. Lesnic), j.niesen@leeds.ac.uk (J. Niesen).

**Abstract**

**Purpose** – The present research is aimed at numerically retrieving five constant dimensional thermo-physical properties of a biological tissue from dimensionless boundary temperature measurements.

**Design/methodology/approach** – The thermal-wave model of bio-heat transfer is used as an appropriate model because of its realism in situations in which the heat flux is extremely high or low and imposed over a short duration of time. For the numerical discretization, an unconditionally stable finite difference scheme used as a direct solver is developed. The sensitivity coefficients of the dimensionless boundary temperature measurements with respect to five constant dimensionless parameters appearing in a non-dimensionalized version of the governing hyperbolic model are computed. The retrieval of those dimensionless parameters, from both exact and noisy measurements, is successfully achieved using a minimization procedure based on the MATLAB optimization toolbox routine *lsqnonlin*. The values of the five dimensional parameters are recovered by inverting a non-linear system of algebraic equations connecting those parameters to the dimensionless parameters whose values have already been recovered.

**Findings** – Accurate and stable numerical solutions for the unknown thermo-physical properties of a biological tissue from dimensionless boundary temperature measurements are obtained using the proposed numerical procedure.

**Research limitations/implications** – The current investigation is limited to the retrieval of constant physical properties, but future work will investigate the reconstruction of the space-dependent blood perfusion coefficient.

**Practical implications** – Since noise inherently present in practical measurements is inverted, the paper is of practical significance and models a real-world situation.

**Social implications** – The findings of the present article are of considerable significance

and interest to practitioners in the biomedical engineering and medical physics sectors.
**Originality/value** – In comparison to Alkhwaji et al. (2012), the novelty and contribution of this work are: (i) considering the more general and realistic thermal-wave model of bio-heat transfer, accounting for a relaxation time, (ii) allowing for the tissue to have a finite size, and (iii) the reconstruction of five thermally significant dimensional parameters.
**Keywords** Identification problem; hyperbolic equation; thermal-wave model; bio-heat transfer
**Paper type** Research paper

# 1 Introduction

The knowledge of the spatio-temporal temperature profile of a living biological tissue is vital for various biomedical applications, including cancer treatment using cryosurgery or hyperthermia therapy in which the elimination of cancer cells is maximized and the damage to the surrounding healthy tissue is minimized (Zhang et al., 2017). In addition, direct measurements of the thermal properties often fail due to their high cost, inefficiency or other technical reasons (Narasimhan and Sadasivam, 2013). Thus, mathematical modelling has become crucial in pre-treatment planning for obtaining the thermo-physical properties and the temperature distribution of the tissue under treatment to be used to direct surgeons to determine the conditions of the tissue being treated (Zhang et al., 2017).

In the last few decades, despite of its simplicity, the Pennes' bio-heat model (Pennes, 1948), based on the classical Fourier's law of heat conduction, has attracted considerable interest for its accurate modelling of a number of applications, including the prediction of temperature of tumours embedded in healthy tissue (Zhang et al., 2006), the study of thermal damage caused by burn injury or medical treatment (Nóbrega and Coelho, 2017), and the study of the effects of thermal parameters on the temperature field (Firoozan et al., 2015; Hafid and Lacroix, 2017). Those studies include the development of closed-form analytical solutions (Gao et al., 1995; Kengne and Lakhssassi, 2015) and numerical methods (Cao et al., 2010; Chan, 1992; Zhao et al., 2005). For instance, Kengne and Lakhssassi (2015) solved the parabolic bio-heat transfer model in spherical coordinates by combining the method of separation of variables with the Green's function approach, while Chan (1992) numerically solved the steady-state and transient Pennes' bio-heat model in two and three dimensions using the boundary element method.

On the other hand, few attention has been paid to the study of the thermal-wave model (Liu et al., 1995), which is a more realistic model for bio-heat transfer, in various applications (Ahmadikia et al., 2012; Liu et al., 1999; Zhukovsky and Srivastava, 2017). For example, Ahmadikia et al. (2012) and Liu et al. (1999) solved the thermal-wave model of bio-heat transfer, along with the Pennes' bio-heat model, with constant and transient heat flux boundary conditions using the Laplace transform method and the method of separation of variables, respectively. The paramount importance of the thermal relaxation, accounted for by the thermal-wave model, has been addressed in several studies (Chester, 1963; Hennessy et al., 2019; Nóbrega and Coelho, 2017), e.g. Chester (1963) for gas dynamics and Hennessy

et al. (2019) for nanoparticle melting. Nóbrega and Coelho (2017) studied the prediction of temperature and thermal damage when a laser is applied for cancer treatment and showed that the hyperbolic model of interest accurately approximates the physical results observed in the experimental work of Mitra et al. (1995). Chester (1963) studied the thermal-wave equation analytically and established an equality between the relaxation time and the critical frequency, that is, the value above which heat propagates as wave-like behaviour rather than diffusion-like behaviour.

Concerning inverse problems for bio-heat transfer, a great deal of numerical techniques has been proposed to solve inverse problems for the Pennes' bio-heat model (Bazán et al., 2017; Cao and Lesnic, 2018; Huntul et al., 2018). However, limited attention has been given to inverse problems for the thermal-wave model (Hsu, 2006; Lee et al., 2013; Yang, 2014). For instance, Lee et al. (2013) studied the thermal-wave model and determined the unknown surface heat flux of a living skin tissue from temperature measurements sampled over the tissue using the conjugate gradient method (CGM) coupled with the discrepancy principle.

In this work, we consider the thermal-wave model whose parameters resemble the thermo-physical properties of real tissue and blood, as given in Alkhwaji et al. (2012); Özen et al. (2008), and attempt to recover five constant thermo-physical parameters, that are: the blood perfusion rate $w_b$, the thermal contact resistance $R''$, the thermal conductivity of tissue $k$, the relaxation time $\tau$ and the heat capacity of tissue $C_{\mathrm{t}}$. Such thermo-physical parameters play fundamental roles in the health of human beings. For instance, the perfusion of blood - the volumetric directionless blood flow rate per unit tissue volume - has a significant role for not only wound healing and the spread of tumour, but also for the removal of wastes and the transfer of oxygen and nutrients to cells in biological tissue. In addition, knowing the blood perfusion, decision-making concerned with the treatment of cancer can be improved and a better understanding of the mechanisms of thermal damages due to burn injury or medical treatment can be accomplished. In comparison to Alkhwaji et al. (2012), the novelty and contribution of this work are: (i) considering the more general and realistic thermal-wave model of bio-heat transfer, accounting for a relaxation time, (ii) allowing for the tissue to have a finite size, and (iii) the reconstruction of five thermally significant dimensional parameters, while only two parameters were recovered in Alkhwaji et al. (2012). To our knowledge, the recovery of such parameters has not been attempted in the literature before.

This paper is organized as follows. In Section 1.1, the thermal-wave model of bio-heat transfer is derived in a generic form, along with the Pennes' bio-heat model, while Section 2 introduces the specific model of interest, along with a non-dimensionalized version of it. In Section 3, an unconditionally stable FDM used as a direct solver is discussed, while two numerical optimization techniques for inversion are introduced and discussed in Section 4, along with a comparison between them. In Section 5, the sensitivity coefficients of the dimensionless boundary temperature measurements with respect to five constant non-dimensional parameters are computed. In Section 6, the retrieval of those dimensionless parameters is obtained using a minimization procedure based on the MATLAB optimization toolbox routine *lsqnonlin*, for exact (i.e. $p = 0$) and noisy (for up to $p = 0.1\%$ noise) measurements. Finally, the values of the five dimensional constant thermo-physical parameters, that are: the blood perfusion rate $w_b$, the thermal contact resistance $R''$, the thermal conductivity $k$, the

relaxation time $\tau$ and the heat capacity of tissue $C_{\mathrm{t}}$, arising in the dimensional thermal-wave model of interest, are recovered by inverting a non-linear system of algebraic equations connecting those parameters to the dimensionless parameters whose values have already been recovered. The conclusions are drawn in Section 7.

## 1.1 Derivation of thermal-wave model

When modelling heat transfer in biological bodies, the Pennes' bio-heat diffusive model may become inaccurate for processes where a finite velocity of heat propagation occurs. In this case, a relaxation time is required for a sufficient amount of energy to accumulate and transfer, as evidenced in the experiments of Bertman and Sandiford (1970); Mitra et al. (1995); Peshkov (1960).

The assumption of infinite velocity of propagation intuitively means that the temperature gradient is felt instantaneously at all locations. This assumption is mathematically described as:

$$q(x,t) = -k\nabla T(x,t), \tag{1}$$

where $T$ is the tissue temperature [°C], $q$ is the heat flux [W m$^{-2}$], $k$ is the thermal conductivity of the tissue [W m$^{-1}$K$^{-1}$], $x$ is the distance [m] and $t$ is the time [s].

On the other hand, the heat balance equation reads as (Liu and Xu, 2000; Pennes, 1948):

$$\rho_{\mathrm{t}} c_{\mathrm{t}} \frac{\partial T}{\partial t}(x,t) + \nabla \cdot q(x,t) = w_b \rho_b c_b (T_a - T) + Q_m(x,t) + Q_e(x,t), \tag{2}$$

where $\rho_{\mathrm{t}}$ and $c_{\mathrm{t}}$ represent the density [kg m$^{-3}$] and specific heat [J kg$^{-1}$K$^{-1}$] of the tissue, respectively, $\rho_b$ and $c_b$ represent the density [kg m$^{-3}$] and specific heat [J kg$^{-1}$K$^{-1}$] of the blood, respectively, $w_b$ is the blood perfusion rate [s$^{-1}$], and $T_a$ is the (constant) arterial blood temperature [°C]. The heat source or sink $w_b \rho_b c_b (T_a - T)$, depending on the sign of the difference $T_a - T$, is due to blood flow, while the heat sources $Q_m$ and $Q_e$ are due to metabolism and other external heating, respectively (Liu and Xu, 2000; Pennes, 1948).

Elimination of the heat flux $q$ from the Fourier's law (1) and the heat balance equation (2) yields the Pennes' bio-heat model given by (Pennes, 1948):

$$\rho_{\mathrm{t}} c_{\mathrm{t}} \frac{\partial T}{\partial t} = k\nabla^2 T + w_b \rho_b c_b (T_a - T) + Q_m + Q_e. \tag{3}$$

To account for the finite velocity of propagation observed in bio-heat transfer, Cattaneo (1958) and Vernotte (1958) independently modified the Fourier's law of heat conduction (1) to account for a relaxation time (time-lag) necessary for the creation of heat flux after a temperature gradient has been imposed. This is mathematically described as:

$$q(x, t+\tau) = -k\nabla T(x,t), \tag{4}$$

where $\tau = \alpha/\mathrm{c}^2$ is the relaxation time [s] necessary for the tissue to respond to the heat perturbation (Özen et al., 2008), $\alpha = k/(\rho_{\mathrm{t}} c_{\mathrm{t}})$ stands for the thermal diffusivity of the tissue [m$^2$ s$^{-1}$], and c denotes the velocity of thermal waves in the biological tissue [m s$^{-1}$] (Mitra et al., 1995).

A first-order Taylor approximation of $q$ in the left-hand side of the modified version of the Fourier's law (4) yields that:

$$q(x,t) + \tau \frac{\partial q}{\partial t}(x,t) = -k \nabla T(x,t). \tag{5}$$

Elimination of the heat flux $q$ from the non-Fourier's law (5) and the heat balance equation (2) yields the thermal-wave model of bio-heat transfer (or sometimes called the Cattaneo-Vernotte equation) given by (Liu et al., 1995; Mochnacki and Tuzikiewicz, 2016):

$$\rho_{\mathrm{t}} c_{\mathrm{t}} \tau \frac{\partial^2 T}{\partial t^2} + (\rho_{\mathrm{t}} c_{\mathrm{t}} + \tau w_b \rho_b c_b) \frac{\partial T}{\partial t} = k \nabla^2 T + w_b \rho_b c_b (T_a - T) + Q_m + Q_e + \tau \frac{\partial}{\partial t}(Q_m + Q_e). \tag{6}$$

It can be noted that when there is no relaxation time, i.e. $\tau = 0$, the thermal-wave hyperbolic model given above coincides with the Pennes' bio-heat parabolic model given by (3).

The objective of the paper is to investigate the governing hyperbolic partial differential equation given by (6) subject to appropriate initial and boundary conditions, when some of the physical coefficients are known or unknown. Those unknown coefficients determining the thermo-physical properties of the tissue and blood are of significance for surgeons to judge the conditions of their patients before undergoing surgeries (Zhang et al., 2017).

The next section introduces the specific model of interest.

# 2 Mathematical formulation

We consider the physical situation investigated in (Alkhwaji et al., 2012) consisting of a blood perfusion measurement using a combined heat flux and temperature (CHFT) sensor that is in thermal contact with the skin tissue. In this experiment, a set of air jets are impinging on the top side of the CHFT sensor creating a sudden increase in convection, which in turn it gives rise to an increase in heat transfer from the surface of the tissue through the sensor. The heat flux and temperature at the surface between the tissue and sensor are measured experimentally, as a function of time. As in Alkhwaji et al. (2012), we assume that the heat transfer is one-dimensional (since the air penetration depth is small compared to the lateral size of the sensor) and that the heat source due to metabolism can be neglected (since it is small compared to the typical heat flux or, if we would be dealing with an ex-vivo tissue). Then, letting $L$ [m] denote the length of the finite tissue slab and $t_{\mathrm{f}}$ [s] a time duration of the thermal process (and assuming, for simplicity, that there is no an external heat source, i.e. $Q_e = 0$), equation (6) simplifies into (Özen et al., 2008):

$$C_{\mathrm{t}} \tau \frac{\partial^2 \theta}{\partial t^2}(x,t) + \big(C_{\mathrm{t}} + \tau w_b C_b\big) \frac{\partial \theta}{\partial t}(x,t) = k \frac{\partial^2 \theta}{\partial x^2}(x,t) - w_b C_b \theta(x,t), \qquad (x,t) \in Q_{t_{\mathrm{f}}} \coloneqq (0,L) \times (0, t_{\mathrm{f}}], \tag{7}$$

where $C_{\mathrm{t}} \coloneqq \rho_{\mathrm{t}} c_{\mathrm{t}}$ [J m$^{-3}$K$^{-1}$] and $C_b \coloneqq \rho_b c_b$ [J m$^{-3}$K$^{-1}$] are the heat capacity of the tissue and blood, respectively, and $\theta = T - T_a$. As $\tau \searrow 0$ equation (7) reduces to the traditional Pennes' equation given by (3).

The downstream side $x = L$ of the sample tissue is assumed insulated, whilst at the surface $x = 0$ of the tissue there is a convective thermal contact with the ambient environment. This results in the following boundary conditions:

$$q(0,t) + \tau \frac{\partial q}{\partial t}(0,t) = -k \frac{\partial \theta}{\partial x}(0,t) = \frac{1}{R''}\big(\theta_s(t) - \theta(0,t)\big), \qquad \frac{\partial \theta}{\partial x}(L,t) = 0, \quad t \in [0, t_{\mathrm{f}}], \quad (8)$$

where $\theta_s(t)$ is the contact skin temperature [°C] measured by the sensor and $R''$ is the thermal contact resistance [$\mathrm{m^2K\ W^{-1}}$], which is the reciprocal of the thermal contact conductance, or the heat transfer coefficient, between the sensor and the skin tissue. The first boundary condition in (8) represents the generalized Newton's law, (Hennessy et al., 2019).

Before the thermal process is initiated, the tissue temperature is at steady-state. In this case, the initial conditions given by (11) below are found by solving the steady-state form of the governing equation given by (7), that is, the second-order ordinary differential equation (ODE) given by:

$$k \frac{d^2 \hat{\theta}}{dx^2}(x) = w_b C_b \hat{\theta}(x), \quad x \in (0, L), \quad (9)$$

subject to the mixed boundary conditions:

$$-k\ \frac{d\hat{\theta}}{dx}(0) = \frac{1}{R''}\big(\theta_{s,0} - \hat{\theta}(0)\big), \qquad \frac{d\hat{\theta}}{dx}(L) = 0, \quad (10)$$

where $\theta_{s,0} = \theta_s(0)$ is the steady-state skin contact temperature [°C]. On solving (9) and (10) results in the initial conditions:

$$\theta(x,0) = \frac{\theta_{s,0}}{D}\left[e^{(x-2L)\sqrt{w_b C_b/k}} + e^{-x\sqrt{w_b C_b/k}}\right], \qquad \frac{\partial \theta}{\partial t}(x,0) = 0, \quad x \in [0, L], \quad (11)$$

where $D = 1 + R'' k\sqrt{w_b C_b/k} + (1 - R'' k\sqrt{w_b C_b/k}) e^{-2L\sqrt{w_b C_b/k}}$.

In comparison to the bioheat conduction model of (Alkhwaji et al., 2012) our mathematical formulation is more general and realistic in the sense that: (i) it allows for the tissue to have a finite size, i.e. $L < \infty$, and (ii) it incorporates the time-lag $\tau > 0$ to take into account for the finite speed of heat wave propagation. Moreover, in (Alkhwaji et al., 2012) only the thermal contact resistance $R''$ and the blood perfusion rate $w_b$ were obtained, whilst in the present study we attempt to retrieve in addition the tissue's thermal conductivity $k$, and heat capacity $C_{\mathrm{t}}$, along with the relaxation time $\tau$.

The next subsection provides the constant thermo-physical properties appearing in the thermal-wave model given by equations (7), (8) and (11) used to model heat transfer in the one-layered, one-dimensional tissue slab, as given in Alkhwaji et al. (2012); Özen et al. (2008).

## 2.1 Thermo-physical properties

The constant thermo-physical properties of the one-layered, one-dimensional slab of the living biological tissue through which heat propagation is modelled by the thermal-wave

model given by equations (7), (8) and (11) are provided in Table 1, as given in Alkhwaji et al. (2012); Özen et al. (2008). In addition, the piecewise constant skin contact temperature $\theta_s(t)$ for $t \in [0, t_{\mathrm{f}}]$, as measured in Alkhwaji et al. (2012), is shown in Figure 1.

Table 1: Values of the constant thermo-physical properties from Alkhwaji et al. (2012), except for $\tau$ from Özen et al. (2008). Note that 1W=1J $\mathrm{s}^{-1}$.

| Symbol | Parameter | Value | Unit |
|---|---|---|---|
| $k$ | Thermal conductivity of the tissue | 0.5 | W $\mathrm{m}^{-1}\mathrm{K}^{-1}$ |
| $\rho_{\mathrm{t}}$ | Density of the tissue | 1050 | kg $\mathrm{m}^{-3}$ |
| $c_{\mathrm{t}}$ | Specific heat of the tissue | 3800 | J $\mathrm{kg}^{-1}\mathrm{K}^{-1}$ |
| $C_{\mathrm{t}}$ | Heat capacity of the tissue, $C_{\mathrm{t}} = \rho_{\mathrm{t}} c_{\mathrm{t}}$ | $3.99 \times 10^6$ | J $\mathrm{m}^{-3}\mathrm{K}^{-1}$ |
| $\rho_b$ | Density of the blood | 1050 | kg $\mathrm{m}^{-3}$ |
| $c_b$ | Specific heat of the blood | 3800 | J $\mathrm{kg}^{-1}\mathrm{K}^{-1}$ |
| $C_b$ | Heat capacity of the blood, $C_b = \rho_b c_b$ | $3.99 \times 10^6$ | J $\mathrm{m}^{-3}\mathrm{K}^{-1}$ |
| $w_b$ | Blood perfusion rate | 0.04 | $\mathrm{s}^{-1}$ |
| $\tau$ | Relaxation time on the heat flux | 20 | s |
| $R''$ | Thermal contact resistance between the tissue and the environment | 0.002 | $\mathrm{m}^2\mathrm{K}$ $\mathrm{W}^{-1}$ |
| $L$ | Length of the one-layered tissue slab | 0.02 | m |
| $t_{\mathrm{f}}$ | Time duration of the thermal process | 60 | s |

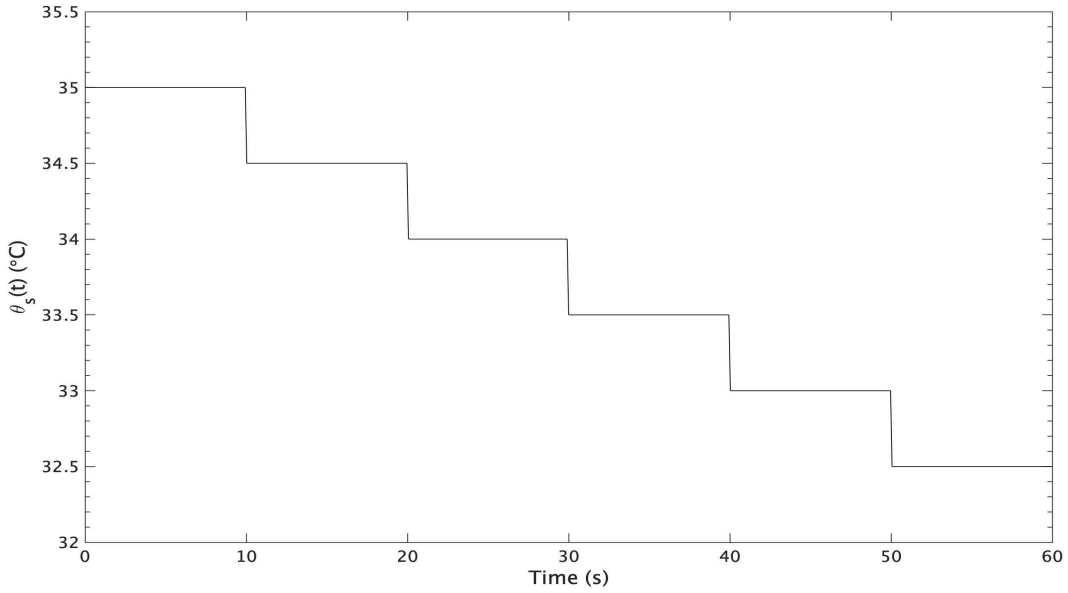


Figure 1: Skin contact temperature $\theta_s(t)$ for $t \in [0, t_{\mathrm{f}}]$, when $t_{\mathrm{f}} = 60$ s.

The next subsection presents a non-dimensionalized version of the thermal-wave model given by equations (7), (8) and (11).

## 2.2 Dimensionless model

Non-dimensionalization is a useful procedure utilized in various sub-fields of Applied Mathematics such as Fluid Dynamics, Thermoelasticity and Heat Transfer to remove the units of variables and to reduce the number of parameters of the models for numerical convenience. We introduce the following change of variables:

$$\bar{x} = \frac{x}{L}, \qquad \bar{t} = \frac{t}{t_{\mathrm{f}}}, \qquad \bar{\theta}(\bar{x}, \bar{t}) = \frac{\theta(x,t)}{\theta_{s,0}}, \qquad \bar{\theta}_s(\bar{t}) = \frac{\theta_s(t)}{\theta_{s,0}}. \tag{12}$$

Then, the dimensionless form of the thermal-wave model given by equations (7), (8) and (11) (omitting the bars for clarity) can be written as:

$$\frac{\partial^2\theta}{\partial t^2}(x,t) + a_1\frac{\partial\theta}{\partial t}(x,t) = a_2\frac{\partial^2\theta}{\partial x^2}(x,t) - a_3\theta(x,t), \quad (x,t) \in \big(0,1\big) \times \big(0,1\big], \tag{13}$$

subject to the initial conditions:

$$\theta(x,0) = \frac{1}{D}\left[e^{a_5(x-2)} + e^{-a_5 x}\right], \qquad \frac{\partial\theta}{\partial t}(x,0) = 0, \quad x \in [0,1], \tag{14}$$

and the mixed boundary conditions:

$$-a_4\frac{\partial\theta}{\partial x}(0,t) = \theta_s(t) - \theta(0,t), \qquad \frac{\partial\theta}{\partial x}(1,t) = 0, \quad t \in \big[0,1\big], \tag{15}$$

where

$$a_1 = \frac{t_{\mathrm{f}}}{\tau} + \frac{w_b C_b t_{\mathrm{f}}}{C_{\mathrm{t}}}, \quad a_2 = \frac{k t_{\mathrm{f}}^2}{\tau C_{\mathrm{t}} L^2}, \quad a_3 = \frac{w_b C_b t_{\mathrm{f}}^2}{\tau C_{\mathrm{t}}}, \quad a_4 = \frac{R'' k}{L}, \quad a_5 = \sqrt{\frac{w_b C_b}{k}}L, \tag{16}$$

and the constant $D$ can be written as $D = 1 + a_4 a_5 + (1 - a_4 a_5)e^{-2a_5}$.

In the next section, an unconditionally stable FDM used as a direct solver is discussed, along with a convergence test for verification of the proposed direct solver.

# 3 Numerical solution of direct problem

Let us consider a generic hyperbolic problem given by:

$$a\frac{\partial^2 u}{\partial t^2}(x,t) + b\frac{\partial u}{\partial t}(x,t) = c\frac{\partial^2 u}{\partial x^2}(x,t) - du(x,t) + f(x,t), \quad (x,t) \in Q_{t_{\mathrm{f}}}, \tag{17}$$

where $a, b, c$ and $d$ are given positive constants, and $f$ is a given force function, subject to the initial conditions:

$$u(x,0) = \phi(x), \qquad \frac{\partial u}{\partial t}(x,0) = \psi(x), \quad x \in [0,L], \tag{18}$$

where $\phi$ and $\psi$ are prescribed functions, and the Robin boundary conditions:

$$\alpha_1 u(0,t) + \beta_1\frac{\partial u}{\partial x}(0,t) = R_1(t), \qquad \alpha_2 u(L,t) + \beta_2\frac{\partial u}{\partial x}(L,t) = R_2(t), \quad t \in [0,t_{\mathrm{f}}], \tag{19}$$

where $\alpha_i$ and $\beta_i \neq 0$ are prescribed constants, and $R_i$ are prescribed functions for $i = 1, 2$.

We introduce an intermediate variable $v$ (Dai and Nassar, 1999) as:

$$v \coloneqq au_t + bu, \quad (x,t) \in Q_{t_\mathrm{f}}, \tag{20}$$

then:

$$v_t = cu_{xx} - du + f(x,t), \quad (x,t) \in Q_{t_\mathrm{f}}. \tag{21}$$

From (18) and (20) we obtain the initial condition:

$$v(x,0) = a\psi(x) + b\phi(x), \quad x \in [0, L]. \tag{22}$$

We subdivide the computational domain $Q_{t_\mathrm{f}}$ into $M$ and $N$ subintervals of equal mesh size $\Delta x = L/M$ and uniform time step $\Delta t = t_\mathrm{f}/N$, respectively. At the grid node $(x_i, t_j)$, we denote $u_{i,j} \coloneqq u(x_i, t_j)$, $v_{i,j} \coloneqq v(x_i, t_j)$ and $f_{i,j} \coloneqq f(x_i, t_j)$, where $x_i = i\Delta x$ and $t_j = j\Delta t$ for $i = \overline{0, M}$ and $j = \overline{0, N}$.

The Crank-Nicolson method, which is unconditionally stable and second-order accurate, discretizes (20), (21), (18), (22) and (19) as:

$$\frac{u_{i,j+1} - u_{i,j}}{\Delta t} = \frac{1}{2a}\big(v_{i,j} - bu_{i,j} + v_{i,j+1} - bu_{i,j+1}\big), \tag{23}$$

$$\frac{v_{i,j+1} - v_{i,j}}{\Delta t} = \frac{1}{2}\left(\frac{c}{(\Delta x)^2}\delta_x^2 u_{i,j} - du_{i,j} + f_{i,j} + \frac{c}{(\Delta x)^2}\delta_x^2 u_{i,j+1} - du_{i,j+1} + f_{i,j+1}\right), \tag{24}$$

$$i = \overline{0, M}, \quad j = \overline{0, (N-1)},$$

$$u_{i,0} = \phi(x_i), \qquad v_{i,0} = a\psi(x_i) + b\phi(x_i), \quad i = \overline{0, M}, \tag{25}$$

$$\alpha_1 u_{0,j} + \beta_1 \frac{u_{1,j} - u_{-1,j}}{2\Delta x} = R_1(t_j), \qquad \alpha_2 u_{M,j} + \beta_2 \frac{u_{M+1,j} - u_{M-1,j}}{2\Delta x} = R_2(t_j), \quad j = \overline{0, N}, \tag{26}$$

where $u_{-1,j} = u(-\Delta x, t_j)$ and $u_{M+1,j} = u(L + \Delta x, t_j)$ for $j = \overline{0, N}$ and $\delta_x^2 u_{i,j} = u_{i-1,j} - 2u_{i,j} + u_{i+1,j}$.

Solving (23) for $v_{i,j+1}$, we obtain:

$$v_{i,j+1} = \left(b + \frac{2a}{\Delta t}\right)u_{i,j+1} + \left(b - \frac{2a}{\Delta t}\right)u_{i,j} - v_{i,j}. \tag{27}$$

Introducing (27) in (24), we obtain:

$$-Au_{i-1,j+1} + Bu_{i,j+1} - Au_{i+1,j+1} = Au_{i-1,j} + Cu_{i,j} + Au_{i+1,j} + 2v_{i,j} + \frac{\Delta t}{2}\big(f_{i,j} + f_{i,j+1}\big), \tag{28}$$

for $i = \overline{0, M}$, $j = \overline{0, (N-1)}$, where $A = \dfrac{c\Delta t}{2(\Delta x)^2}$, $B = \left(\dfrac{2a}{\Delta t} + b\right) + \dfrac{c\Delta t}{(\Delta x)^2} + \dfrac{d\Delta t}{2}$ and $C = \left(\dfrac{2a}{\Delta t} - b\right) - \left(\dfrac{c\Delta t}{(\Delta x)^2} + \dfrac{d\Delta t}{2}\right)$.

At each time step $t_{j+1} = (j+1)\Delta t$ for $j = \overline{0, (N-1)}$, using the discretized Robin boundary conditions given by (26), the difference equations given by (27) and (28) can be reformulated as a two-step implicit FDM procedure of the form:

$$\tilde{L}\boldsymbol{u_{j+1}} = \tilde{E}\boldsymbol{u_j} + 2\boldsymbol{v_j} + \tilde{\boldsymbol{b}}^{\boldsymbol{j}}, \tag{29}$$

$$\boldsymbol{v_{j+1}} = \left(b + \frac{2a}{\Delta t}\right)\boldsymbol{u_{j+1}} + \left(b - \frac{2a}{\Delta t}\right)\boldsymbol{u_j} - \boldsymbol{v_j}, \tag{30}$$

where:

$$\boldsymbol{u_j} = (u_{0,j}, \ldots, u_{M,j})^{\mathrm{T}}, \quad \boldsymbol{v_j} = (v_{0,j}, \ldots, v_{M,j})^{\mathrm{T}},$$

$$\tilde{L} = \begin{pmatrix} B-\lambda_1 & -2A & 0 & \ldots & 0 & 0 & 0 \\ -A & B & -A & \ldots & 0 & 0 & 0 \\ \vdots & \vdots & \vdots & \ddots & \vdots & \vdots & \vdots \\ 0 & 0 & 0 & \ldots & -A & B & -A \\ 0 & 0 & 0 & \ldots & 0 & -2A & B+\lambda_2 \end{pmatrix},$$

$$\tilde{E} = \begin{pmatrix} C+\lambda_1 & 2A & 0 & \ldots & 0 & 0 & 0 \\ A & C & A & \ldots & 0 & 0 & 0 \\ \vdots & \vdots & \vdots & \ddots & \vdots & \vdots & \vdots \\ 0 & 0 & 0 & \ldots & A & C & A \\ 0 & 0 & 0 & \ldots & 0 & 2A & C-\lambda_2 \end{pmatrix},$$

$$\tilde{\boldsymbol{b}}^{\boldsymbol{j}} = \begin{pmatrix} \frac{\Delta t}{2}\big(f_{0,j} + f_{0,j+1}\big) - \frac{2A\Delta x}{\beta_1}\big(R_1(t_j) + R_1(t_{j+1})\big) \\ \frac{\Delta t}{2}(f_{1,j} + f_{1,j+1}) \\ \vdots \\ \frac{\Delta t}{2}(f_{M-1,j} + f_{M-1,j+1}) \\ \frac{\Delta t}{2}(f_{M,j} + f_{M,j+1}) + \frac{2A\Delta x}{\beta_2}\big(R_2(t_j) + R_2(t_{j+1})\big) \end{pmatrix},$$

and $\lambda_k = \dfrac{2\alpha_k A\Delta x}{\beta_k}$ for $k = 1, 2$.

We next consider a numerical example to verify the convergence and accuracy of the proposed FDM scheme.

**Example.** We consider the direct problem (17)-(19) with $t_{\mathrm{f}} = L = 1$, $a = b = c = d = 1$, $\alpha_i = \beta_i = 1$ for $i = 1, 2$,

$$u(x,0) = \phi(x) = \cos(\pi x) + \sin(\pi x) + 2, \qquad \frac{\partial u}{\partial t}(x,0) = \psi(x) = \cos(\pi x) + 2, \tag{31}$$

$$R_1(t) = \pi + 3e^t, \qquad R_2(t) = e^t - \pi, \tag{32}$$

and

$$f(x,t) = (3+\pi^2)e^t\cos(\pi x) + (1+\pi^2)\sin(\pi x) + 6e^t. \tag{33}$$

Then, the analytical solution is given by:

$$u(x,t) = e^t\big(\cos(\pi x) + 2\big) + \sin(\pi x). \tag{34}$$

Figure 2 shows the analytical (34) and numerical solutions obtained with various mesh sizes $M = N \in \{10, 20, 40\}$. The absolute errors between the exact and numerical FDM solutions are also included. From this figure, it can be seen that the convergence of the

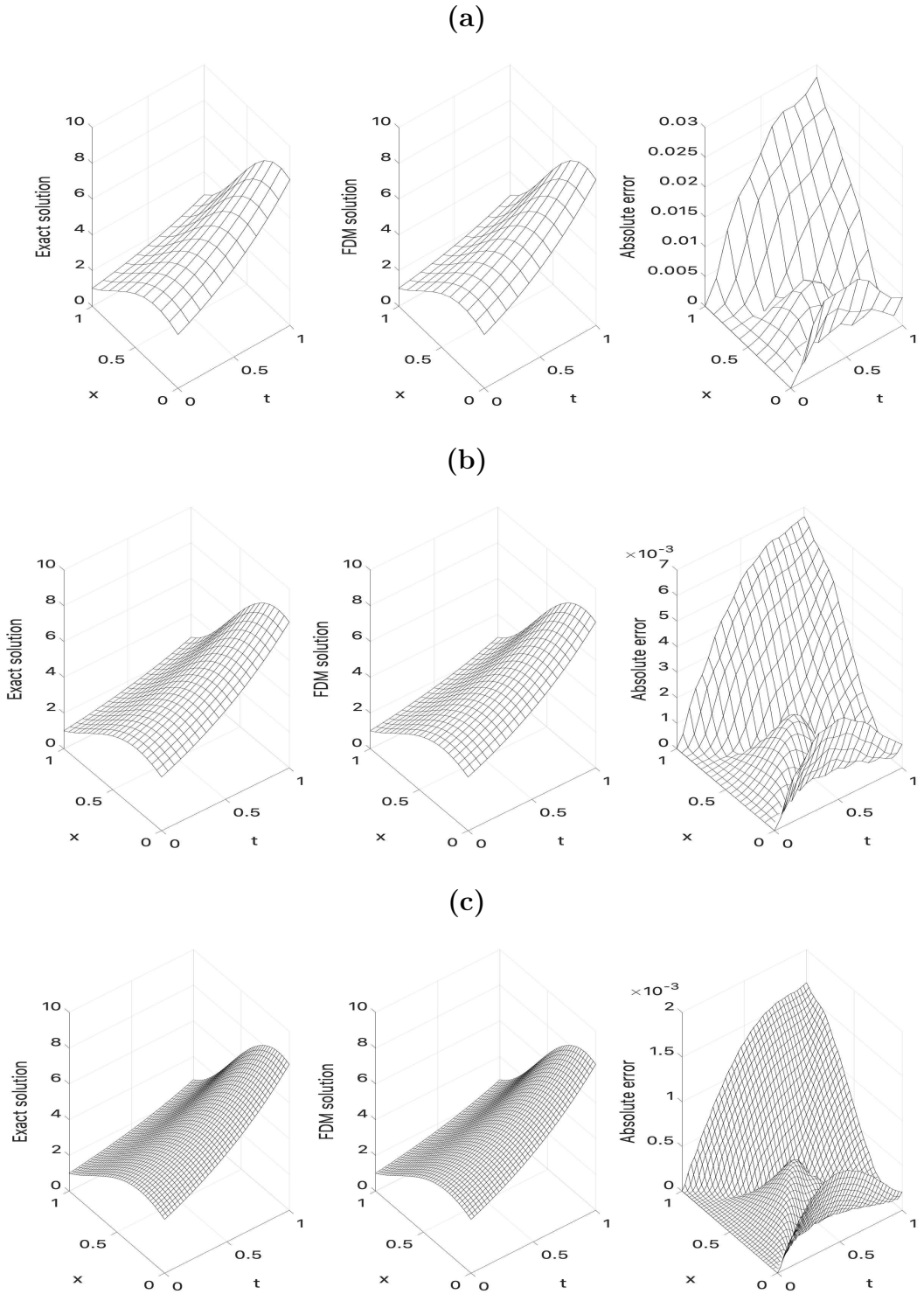


Figure 2: The analytical (34) and numerical FDM solutions for the temperature $u(x,t)$ of the direct problem (17)-(19) obtained with various mesh sizes: (a) $M = N = 10$, (b) $M = N = 20$, and (c) $M = N = 40$. The absolute errors between them are also included.

numerical FDM solution towards the analytical solution (34) is achieved since the absolute error approaches zero as the mesh size is refined.

In the next section, we introduce two numerical optimization techniques for inversion. In addition, we numerically simulate the generalized heat flux at $x = 0$,

$$-k\frac{\partial\theta}{\partial x}(0,t) =: \tilde{q}(t) = q(0,t) + \tau\frac{\partial q}{\partial t}(0,t), \quad t \in [0, t_{\mathrm{f}}], \tag{35}$$

by solving the dimensional model given by equations (7), (8) and (11), and the dimensionless boundary temperatures at $x \in \{0, 1\}$ by solving the dimensionless model given by equations (13)-(15), to be used as additional measurements for a comparison between the presented inversion techniques and for the reconstruction of all possible parameters of the dimensionless model given by equations (13)-(15), respectively.

# 4 Numerical solution of inverse problems

A discussion of two numerical optimization approaches for inversion is performed in the next two subsections.

## 4.1 Graphical approach

The idea of this approach is to visualize the objective function associated with the inverse problem under consideration and then find its minimum and its corresponding minimizers graphically. We apply this method for the determination of one or two parameters simultaneously. As for the reconstruction of more than two parameters, this graphical method becomes impractical and hence the second inversion approach described next is more efficient.

## 4.2 MATLAB optimization toolbox routine *lsqnonlin*

We employ the MATLAB optimization toolbox routine *lsqnonlin*, which does not require supplying by the user the gradient of the objective function associated (Mathworks, 2012). This routine attempts to find the minimum of a sum of squares by starting from an arbitrary initial guess. This routine is compiled with the following parameters:

- Algorithm is the Trust Region Reflective (TRR) minimization (Coleman and Li, 1996).
- Maximum number of iterations = $10^2 \times$ (number of variables).
- Maximum number of objective function evaluations = $10^2 \times$ (number of variables).
- Termination tolerance on the function value = $10^{-20}$.
- Solution tolerance = $10^{-20}$.
- Lower and upper bounds on the unknowns = $10^{-10}$ and $10^3$, respectively.

- Initial guesses for the unknowns = unity.

In the next subsection, we numerically simulate the generalized heat flux (35) of the dimensional model given by equations (7), (8) and (11), and the dimensionless boundary temperatures of the dimensionless model given by equations (13)-(15), to be used as additional measurements for a comparison between the presented inversion techniques discussed in Sections 4.1 and 4.2, respectively, and for the reconstruction of all possible parameters of the dimensionless model given by equations (13)-(15), respectively. It is worth pointing out that, according to (35), in the hyperbolic model of bioheat transfer that is considered in this paper, the temperature gradient is not the heat flux $q(0,t)$ but the generalized heat flux $\tilde{q}(t) \coloneqq q(0,t) + \tau \partial_t q(0,t)$, (Yu, 2018).

## 4.3 Exact and noisy measurements

As for as the generalized heat flux used in the inversion of the model parameters as input data coming from experiment, in practice, it would be actually the heat flux $q(0,t)$ that we would measure with some error $\varepsilon > 0$. Then, we could compute the time-derivative using a finite-difference approximation with a step size of $\mathcal{O}(\sqrt{\varepsilon})$ for stability, and finally, if $\tau$ is known, we could have the generalized heat flux $\tilde{q}(t)$ calculated by adding $q(0,t)$ to $\tau \dfrac{\partial q}{\partial t}(0,t)$, as defined in (35). However, in this paper we simulate the data $\tilde{q}(t)$ numerically by solving, using the FDM described in Section 3, the direct problem given by equations (7), (8) and (11), with the model parameters of Table 1, to provide the value of $-k\partial_x\theta(0,t)$. In any case, the generalized flux measurements are only used in section 4.4 to illustrate the comparison between the two inversion approaches; the real inversion performed in Section 6 uses instead non-destructive testing measurements of the boundary temperature, which are also practically feasible and realistic. The dimensional generalized heat flux $\tilde{q}(t) = -k\partial_x\theta(0,t)$, and the dimensionless boundary temperatures $\theta(0,t)$ and $\theta(1,t)$ are depicted in Figure 3 for various mesh sizes $M = N \in \{160, 320, 640\}$, showing that convergent results have been achieved. The dimensional boundary temperatures can easily be inferred from Figures 3(b) and (c) and equation (12) by multiplying the dimensionless time $\bar{t}$ by $t_{\mathrm{f}} = 60$ s and the dimensionless temperature $\bar{\theta}$ by $\theta_{s,0} = 35$°C.

In what follows, in order to avoid committing an inverse crime, we consider the numerically simulated dimensional generalized heat flux $\tilde{q}(t)$, and the dimensionless boundary temperatures $\theta(0,t)$ and $\theta(1,t)$ obtained with $M = N = 640$ from our FDM direct solver as input data in the inverse problems of interest, which themselves are solved with a coarser mesh of $M_{\mathrm{inv}} = N_{\mathrm{inv}} = 320$. Further, since in reality measured data is subject to noise, we perturb the numerically simulated data by random noise as:

$$\tilde{q}^{\epsilon}(t_j) = \tilde{q}(t_j) + \epsilon 1_j, \quad j = \overline{1, N_{\mathrm{inv}}}, \tag{36}$$

$$\theta^{\epsilon}(0,t_j) = \theta(0,t_j) + \epsilon 2_j, \quad j = \overline{1, N_{\mathrm{inv}}}, \tag{37}$$

$$\theta^{\epsilon}(1,t_j) = \theta(1,t_j) + \epsilon 3_j, \quad j = \overline{1, N_{\mathrm{inv}}}, \tag{38}$$

where $\epsilon 1_j$, $\epsilon 2_j$ and $\epsilon 3_j$ are random variables generated from a Gaussian normal distribution

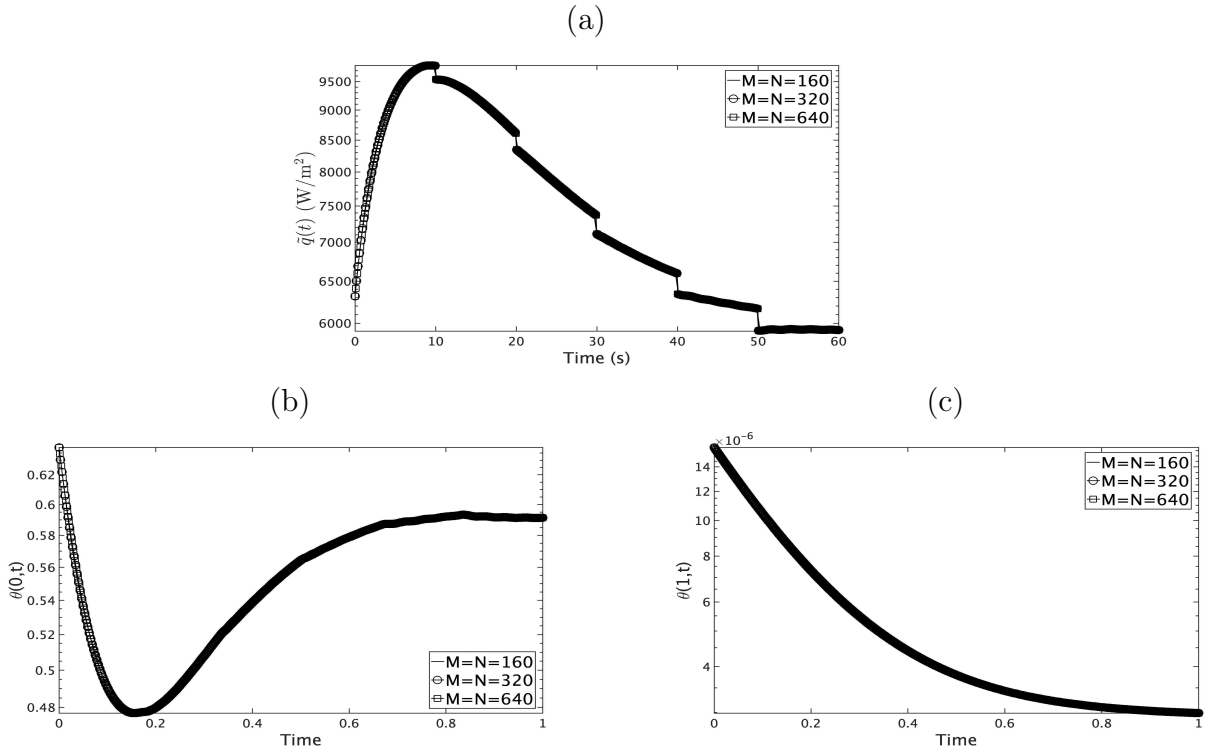


Figure 3: Plots of the simulated (a) dimensional generalized heat flux $\tilde{q}(t)$ at $x = 0$, (b) dimensionless boundary temperature $\theta(0, t)$ at $x = 0$, and (c) dimensionless boundary temperature $\theta(1, t)$ at $x = 1$.

with mean zero and standard deviations $\sigma_1$, $\sigma_2$ and $\sigma_3$, respectively, given by:

$$\sigma_1 = p \times \max_{j=\overline{1,N_{\text{inv}}}} |\tilde{q}(t_j)|, \quad \sigma_2 = p \times \max_{j=\overline{1,N_{\text{inv}}}} |\theta(0,t_j)|, \quad \sigma_3 = p \times \max_{j=\overline{1,N_{\text{inv}}}} |\theta(1,t_j)|, \tag{39}$$

where $p$ represents the percentage of noise. We use the MATLAB function $normrnd(0, \sigma_k, N_{\text{inv}})$ to generate the random variables $(\epsilon k_j)_{j=\overline{1,N_{\text{inv}}}}$ for $k = 1, 2, 3$.

The relative error (RE%) used to evaluate the accuracy of the numerical results is defined as:

$$\text{RE}(\beta) = \frac{|\beta^{\text{numerical}} - \beta^{\text{exact}}|}{|\beta^{\text{exact}}|} \times 100\%, \tag{40}$$

where $\beta^{\text{numerical}}$ denotes the numerically obtained quantity and $\beta^{\text{exact}}$ stands for the true value of the such quantity, if available. In addition, the average relative error (ERR%) used to evaluate the total accuracy of the numerical results for the reconstruction of the five parameters of interest is defined as:

$$\text{ERR} = \frac{1}{5} \sum_{i=1}^{5} \frac{|\beta_i^{\text{numerical}} - \beta_i^{\text{exact}}|}{|\beta_i^{\text{exact}}|} \times 100\%, \tag{41}$$

where $(\beta_i^{\text{numerical}})_{i=\overline{1,5}}$ denotes a vector of the numerically obtained quantities and $(\beta_i^{\text{exact}})_{i=\overline{1,5}}$ stands for a vector of the true values of such quantities, if available.

The next section presents a comparison between the two numerical optimization approaches discussed in Sections 4.1 and 4.2, respectively, for the reconstruction of one or two parameters simultaneously.

## 4.4 Comparison between two inversion approaches

We illustrate the two numerical optimization approaches discussed in Sections 4.1 and 4.2, respectively, for the reconstruction of one or two parameters simultaneously. We reconstruct the blood perfusion rate $w_b$ alone, as well as the blood perfusion rate $w_b$ and the thermal contact resistance $R''$ simultaneously from the measured generalized flux $\tilde{q}(t_j)$ for $j = \overline{1, N_{\text{inv}}}$, whose convergent results have already been shown in Figure 3(a). The details of the graphical approach, the toolbox *lsqnonlin* routine, the FDM, and the noise and the error computation are the same as described in Sections 4.1–4.3.

The objective functions that we typically minimize for the reconstruction of the blood perfusion rate $w_b$ alone, as well as the blood perfusion rate $w_b$ and the thermal contact resistance $R''$ simultaneously are given, respectively, by:

$$F_1(w_b) = \frac{1}{\sigma_f^2} \sum_{j=1}^{N_{\text{inv}}} \left( \tilde{q}(t_j) - \tilde{q}_c(t_j; w_b) \right)^2, \tag{42}$$

$$F_2(w_b, R'') = \frac{1}{\sigma_f^2} \sum_{j=1}^{N_{\text{inv}}} \left( \tilde{q}(t_j) - \tilde{q}_c(t_j; w_b, R'') \right)^2, \tag{43}$$

where $\tilde{q}_c$ denotes the computed generalized flux and $\sigma_f^2$ is the variance of the noise in the corresponding dimensional generalized flux measurement found using the MATLAB command *var*. In the case of noisy measurement, $\tilde{q}$ is replaced by $\tilde{q}^\epsilon$ (defined in (36)) in (42) and (43).

The convergence of the objective functions $F_1$ and $F_2$ given by (42) and (43), respectively, as functions of the number of iterations, minimized using the MATLAB optimization toolbox routine *lsqnonlin*, is depicted in the top-left and lower-left of Figure 4, respectively, for both exact (i.e. $p = 0$) and noisy (with $p = 1\%$ noise) data, while the top-right and lower-right of the same figure illustrate the graphical approach of Section 4.1 based on simply plotting the objective functions $F_1$ and $F_2$ given by (42) and (43), respectively, for exact data, i.e. $p = 0$, on linear-log scale for $w_b \in [0, 0.08] s^{-1}$ and $R'' \in [1.5, 2.5] \times 10^{-3}$ m$^2$K W$^{-1}$.

Table 2 shows the exact and recovered values of the blood perfusion rate $w_b$ when the generalized heat flux measurement is noise-free or subjected to a noise of level of $p = 1\%$. The numerical values have been obtained using the two numerical optimization approaches discussed in Sections 4.1 and 4.2, respectively. The initial guess for the unknown blood perfusion rate $w_b$ when using the MATLAB routine *lsqnonlin* was taken equal to unity. Other details such as the values of the objective function $F_1$ given by (42) at the recovered solutions, the ideal values of the objective function denoted by $F_1^{\text{ideal}}$ and found by substituting the exact value of the blood perfusion $w_b$ into the direct problem given by equations (7), (8) and (11) and then solving for the generalized heat flux, subsequently used to evaluate the objective function $F_1$, are also included.

Table 3 shows the exact and recovered values of the blood perfusion rate $w_b$ and the thermal contact resistance $R''$ when the generalized heat flux measurement is noise-free or subjected to a noise of level of $p = 1\%$. The numerical values have been obtained using the two numerical optimization approaches discussed in Sections 4.1 and 4.2, respectively. The initial guesses for the unknown blood perfusion rate $w_b$ and the thermal contact resistance $R''$ when using the MATLAB routine *lsqnonlin* were taken equal to unity.

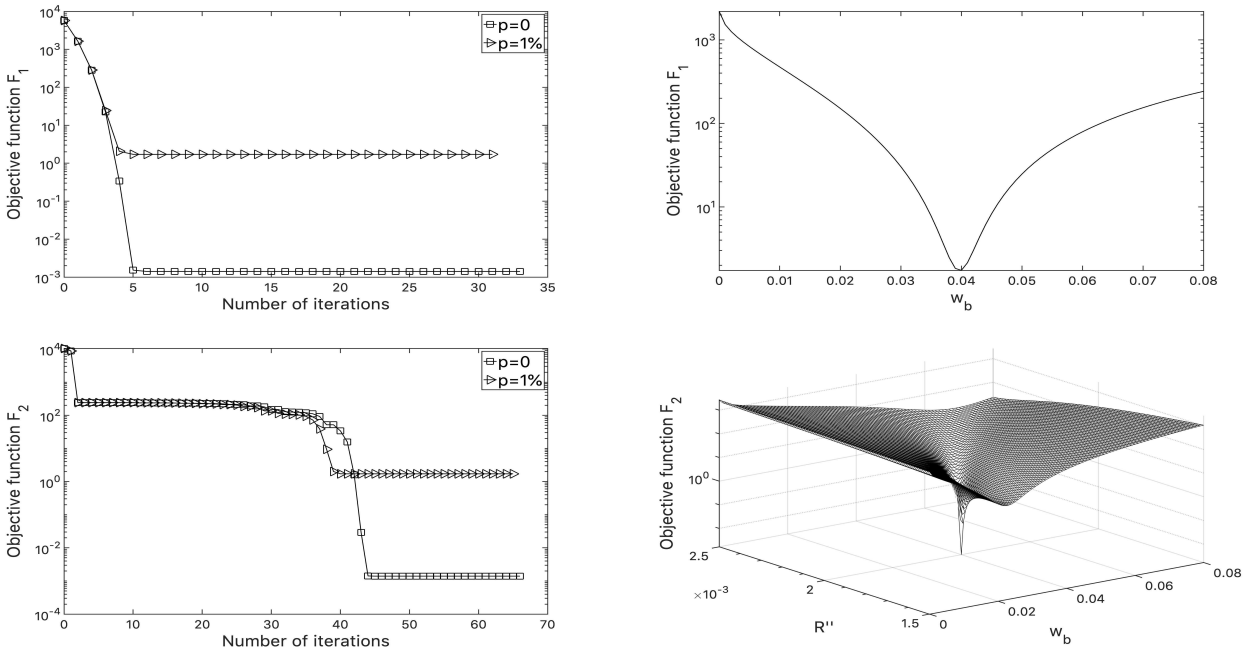


Figure 4: The objective functions $F_1$ and $F_2$ given by (42) and (43), respectively, as functions of the number of iterations, with $p = 1\%$ noise and without ($p = 0$) noise in (36) (left panel), and the graphical representations of the objective functions on linear-log scale, without ($p = 0$) noise (right panel).

Table 2: Recovered values of the blood perfusion rate $w_b$ and the relative errors (RE%).

| Using the graphical approach | | | | | |
|---|---|---|---|---|---|
| | | $p = 0$ | | $p = 1\%$ | |
| | exact | numerical | RE% | numerical | RE% |
| $w_b$ | 0.04 | 0.04 | 0 | 0.04 | 0 |
| Value of objective function $F_1$ | | $1.664\times10^{-3}$ | | 1.738 | |
| Computational time | | 9 seconds | | 10 seconds | |
| Sampling box | | [0, 0.08] | | | |
| Number of sampling nodes | | 81 | | | |
| Using the MATLAB optimization toolbox routine *lsqnonlin* | | | | | |
| | | $p = 0$ | | $p = 1\%$ | |
| | exact | numerical | RE% | numerical | RE% |
| $w_b$ | 0.04 | 0.0399 | 0.08% | 0.0397 | 0.77% |
| $F_1^{\text{ideal}}$ | | $1.664\times10^{-3}$ | | 1.738 | |
| Value of objective function $F_1$ | | $1.409\times10^{-3}$ | | 1.714 | |
| Number of iterations | | 33 | | 31 | |
| Computational time | | 8 seconds | | 9 seconds | |
| Reason of halting iteration | | Norm of current step is less than step tolerance, $10^{-20}$ | | | |

Table 3: Recovered values of the blood perfusion rate $w_b$ and the thermal contact resistance $R''$, and the relative errors (RE%).

| Using the graphical approach | | | | | |
|---|---|---|---|---|---|
| | | $p = 0$ | | $p = 1\%$ | |
| | exact | numerical | RE% | numerical | RE% |
| $w_b$ | 0.04 | 0.04 | 0 | 0.04 | 0 |
| $R''$ | 0.002 | 0.002 | 0 | $2.012\times10^{-3}$ | 0.6% |
| Value of objective function $F_2$ | | $1.664\times10^{-3}$ | | 1.732 | |
| Computational time | | 15 minutes | | 17 minutes | |
| Sampling box | | $[0,\ 0.08]\times[0.0015, 0.0025]$ | | | |
| Number of sampling nodes | | $81\times81$ | | | |
| Using the MATLAB optimization toolbox routine *lsqnonlin* | | | | | |
| | | $p = 0$ | | $p = 1\%$ | |
| | exact | numerical | RE% | numerical | RE% |
| $w_b$ | 0.04 | 0.03995 | 0.12% | 0.0399 | 0.34% |
| $R''$ | 0.002 | $1.999\times10^{-3}$ | 0.02% | $2.004\times10^{-3}$ | 0.20% |
| $F_2^{\text{ideal}}$ | | $1.664\times10^{-3}$ | | 1.738 | |
| Value of objective function $F_2$ | | $1.399\times10^{-3}$ | | 1.713 | |
| Number of iterations | | 66 | | 65 | |
| Computational time | | 21 seconds | | 22 seconds | |
| Reason of halting iteration | | *lsqnonlin* solver exceeded function evaluation limit, 200 | | | |

Nevertheless, a comparison of the computational time shown in Table 3 for the simultaneous reconstruction of the blood perfusion rate $w_b$ and the thermal contact resistance $R''$ using the two numerical optimization approaches discussed in Sections 4.1 and 4.2, respectively, reveals that the graphical method of Section 4.1 becomes inefficient when two or more parameters have to be estimated. In such a situation, the optimization approach of Section 4.2 is employed, as invoked in Section 6 for the reconstruction of all the five dimensionless constant parameters $(a_i)_{i=\overline{1,5}}$ appearing in the non-dimensionalized model given by equations (13)-(15). However, prior to this full inversion, in the next section, it is useful to perform a sensitivity analysis (Beck and Arnold, 1985; Özişik and Orlande, 2000) of the five dimensionless parameters defined in equation (16) appearing in the model given by equations (13)-(15) in order to gain an insight into the amount of information contained in the boundary temperature measurements.

# 5 Sensitivity analysis

In this section, we perform a sensitivity analysis to gain an insight into which parameters have the highest influence on the measured boundary temperatures $\theta(0, t_j)$ and $\theta(1, t_j)$ for

$j = \overline{1, N_{\text{inv}}}$. The sensitivity coefficients can be computed by various approaches, as described in Beck and Arnold (1985); Özişik and Orlande (2000), such as the analytical approach, the boundary value approach and the finite difference approach. We chose the latest to compute the normalized sensitivity coefficients as it is the most direct and appropriate approach for the inverse problem considered in this paper. The normalized sensitivity coefficient of the dimensionless boundary measurement $\theta(j,t)$, $j \in \{0,1\}$, with respect to the parameter $\gamma_i$ is defined as (Beck and Arnold, 1985; Özişik and Orlande, 2000):

$$S_j(\gamma_i)(t) \coloneqq \gamma_i \frac{\partial \theta(j,t)}{\partial \gamma_i} \approx \gamma_i \frac{\theta(j,t;\gamma_1,\cdots,\gamma_i+\Delta\gamma_i,\cdots,\gamma_\rho) - \theta(j,t;\gamma_1,\cdots,\gamma_i,\cdots,\gamma_\rho)}{\Delta\gamma_i}, \quad j \in \{0,1\}, \quad (44)$$

where $\Delta\gamma_i$ is relatively small, e.g. $\Delta\gamma_i = 0.001\gamma_i$, where $\gamma_i$ is the true value of the parameter considered. In general, the sensitivity coefficients are desired to be large and uncorrelated.

Figures 5 and 6 show the timewise variations of the normalized sensitivity coefficients $S_0(a_i)$ and $S_1(a_i)$ for $i = \overline{1,5}$ corresponding to the measured dimensionless boundary temperatures $\theta(0,t)$ and $\theta(1,t)$, respectively, obtained using the forward first-order accurate finite difference defined in equation (44). From Figures 5 and 6, it can be seen that the normalized sensitivity coefficients are uncorrelated. However, from the left-hand side of Figure 6 it can be seen that $S_1(a_i)$ for $i = \overline{1,4}$ are of $O(10^{-6})$, hence small, indicating that, compared to Figure 5 where their counterparts, i.e. $S_0(a_i)$ for $i = \overline{1,4}$, are of $O(10^{-1})$, the dimensionless temperature measurement at the convective boundary $x = 0$ contains more information than the measurement at the insulated boundary $x = 1$, see equation (15).

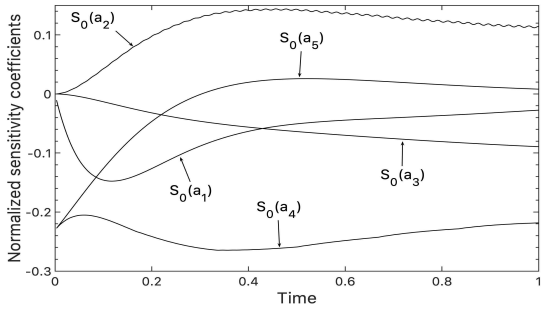


Figure 5: The sensitivity coefficients for the dimensionless boundary temperature $\theta(0,t_j)$ for $j = \overline{1, N_{\text{inv}}}$ with respect to the constant parameters $(a_i)_{i=\overline{1,5}}$.

The MATLAB optimization toolbox routine *lsqnonlin* previously used for the estimation of one or two parameters in Section 4.4 is utilized in the next section to recover all the five dimensionless constant parameters $(a_i)_{i=\overline{1,5}}$ of the dimensionless model given by equations (13)-(15), when both the dimensionless boundary temperatures $\theta(0,t_j)$ and $\theta(1,t_j)$ for $j = \overline{1, N_{\text{inv}}}$ are measured free of noise $p = 0$ or subjected to a noise of level of $p = 0.1\%$. We do not use the generalized heat flux defined in equation (15) as additional measurement because its expression depends on the parameter $a_4$ which is unknown.

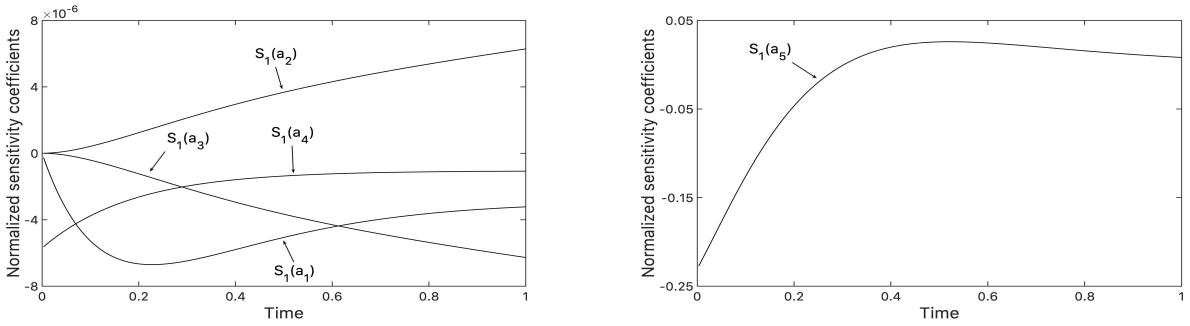


Figure 6: The sensitivity coefficients for the dimensionless boundary temperature $\theta(1,t_j)$ for $j=\overline{1,N_{\rm inv}}$ with respect to the constant parameters $(a_i)_{i=\overline{1,4}}$ (left) and $a_5$ (right).

# 6 Retrieval of five parameters

We herein reconstruct all the five dimensionless constant parameters $\boldsymbol{a}=(a_i)_{i=\overline{1,5}}$ appearing in the dimensionless model given by equations (13)-(15) from the measured dimensionless boundary temperatures $\theta(0,t_j)$ and/or $\theta(1,t_j)$ for $j=\overline{1,N_{\rm inv}}$, whose convergent results have already been shown in Figures 3(b) and (c), respectively. The details of the toolbox *lsqnonlin* routine, the FDM, and the noise and the error computation are the same as described in Sections 4.2 and 4.3.

The objective function that we typically minimize for the reconstruction of all the five dimensionless parameters $\boldsymbol{a}=(a_i)_{i=\overline{1,5}}$ is given by:

$$G(\boldsymbol{a})=G_0(\boldsymbol{a})+G_1(\boldsymbol{a})=\frac{1}{\sigma_0^2}\sum_{j=1}^{N_{\rm inv}}\big(\theta(0,t_j)-\theta_c(0,t_j;\boldsymbol{a})\big)^2+\frac{1}{\sigma_1^2}\sum_{j=1}^{N_{\rm inv}}\big(\theta(1,t_j)-\theta_c(1,t_j;\boldsymbol{a})\big)^2, \quad (45)$$

where:

$$G_0(\boldsymbol{a})=\frac{1}{\sigma_0^2}\sum_{j=1}^{N_{\rm inv}}\big(\theta(0,t_j)-\theta_c(0,t_j;\boldsymbol{a})\big)^2, \quad (46)$$

$$G_1(\boldsymbol{a})=\frac{1}{\sigma_1^2}\sum_{j=1}^{N_{\rm inv}}\big(\theta(1,t_j)-\theta_c(1,t_j;\boldsymbol{a})\big)^2, \quad (47)$$

$\theta_c(0,t_j;\boldsymbol{a})$ and $\theta_c(1,t_j;\boldsymbol{a})$ for $j=\overline{1,N_{\rm inv}}$ denote the computed dimensionless boundary temperatures, and $\sigma_0^2$ and $\sigma_1^2$ are the variances of the noise in the corresponding boundary temperature measurements found using the MATLAB command *var*. In the case of noisy measurements, $\theta(0,t_j)$ and $\theta(1,t_j)$ are replaced by $\theta^\epsilon(0,t_j)$ and $\theta^\epsilon(1,t_j)$ (defined in (37) and (38), respectively), in (45)-(47). The initial guesses for the five unknown dimensionless parameters were taken equal to unity.

Tables 4(a), 4(b) and 5 show the exact and recovered values of all the five dimensionless parameters $(a_i)_{i=\overline{1,5}}$ appearing in the dimensionless model given by equations (13)-(15). Those results have been obtained using the MATLAB optimization toolbox routine *lsqnonlin* when the measurements (noise free, i.e. $p=0$, or with $p=0.1\%$ noise) are only the dimensionless boundary temperature at $x=0$ minimizing (46), the dimensionless boundary

temperature at $x = 1$ minimizing (47), and both the dimensionless boundary temperatures at $x \in \{0, 1\}$ minimizing (45). From Tables 4(a) and (b), it can be seen that the numerical reconstruction of the parameters $a_2$, $a_4$ and $a_5$ are very inaccurate when measuring only the temperature at $x = 0$ or $x = 1$, but a combination of both in the objective function $G$ given by (45) renders the numerically obtained solution for all the five constant parameters $(a_i)_{i=\overline{1,5}}$ accurate, as seen in Table 5. Clearly, there is not enough information when using the individual measurements of $\theta(0, t_j)$ or $\theta(1, t_j)$ for $j = \overline{1, N_{\text{inv}}}$ above and more complementary information is supplied when both these dimensionless boundary temperatures are measured. Other details such as the values of the objective function $G$ given by (45) at the recovered solutions, the ideal values of the objective function denoted by $G^{\text{ideal}}$ and found by substituting the exact values of the five non-dimensional components $(a_i)_{i=\overline{1,5}}$ into the direct problem given by equations (13)-(15) and then solving for the dimensionless boundary temperatures, subsequently used to evaluate the objective function $G$, are also included in Table 5.

The convergence of the objective functions $G_0$, $G_1$ and $G$ given by (46), (47) and (45), respectively, as functions of the number of iterations, corresponding the above three cases, minimized using the MATLAB optimization toolbox routine *lsqnonlin*, is depicted in Figure 7, whilst Figure 8 show the relative errors (RE%) defined in (40) for the unknowns $(a_i)_{i=\overline{1,5}}$ arising in the dimensionless model given by equations (13)-(15) when the measurements are both the dimensionless boundary temperatures at $x \in \{0, 1\}$. From Figure 7(c) as well as Figure 8, it can be seen that the objective function $G$ given by (45) and the relative errors (RE%) defined in (40), as functions of the number of iterations, stabilize in about 40 iterations for both exact and noisy data. Overall from Table 5 and Figure 8, it can be concluded that accurate and stable numerical results have been successfully achieved for the reconstruction of all the five dimensionless constant unknowns $(a_i)_{i=\overline{1,5}}$ appearing in the dimensionless model given by equations (13)-(15).

Table 4: Recovered values of the parameters $(a_i)_{i=\overline{1,5}}$ and the relative errors (RE%) when the measurement is only the dimensionless boundary (a) temperature $\theta(0,t)$ or (b) temperature $\theta(1,t)$.

| (a) When only $\theta(0,t)$ is measured | | | | | |
|---|---|---|---|---|---|
| | | $p=0$ | | $p=0.1\%$ | |
| | exact | numerical | RE% | numerical | RE% |
| $a_1$ | 5.4 | 5.3997 | $5.8\times10^{-3}$% | 5.4052 | 0.1% |
| $a_2$ | 0.05639 | 2.43 | 4209% | 3.29 | 5737% |
| $a_3$ | 7.2 | 7.103 | 1.35% | 7.089 | 1.54% |
| $a_4$ | 0.05 | 0.335 | 570% | 0.394 | 688% |
| $a_5$ | 11.299 | 1.785 | 84% | 1.563 | 86% |
| (b) When only $\theta(1,t)$ is measured | | | | | |
| | | $p=0$ | | $p=0.1\%$ | |
| | exact | numerical | RE% | numerical | RE% |
| $a_1$ | 5.4 | 5.3999 | $1.4\times10^{-3}$% | 5.3988 | 0.02% |
| $a_2$ | 0.05639 | 0.87 | 1442% | 0.85 | 1408% |
| $a_3$ | 7.2 | 35.29 | 390% | 34.54 | 380% |
| $a_4$ | 0.05 | 33.82 | 67548% | 33.73 | 67356% |
| $a_5$ | 11.299 | 6.37 | 44% | 6.37 | 44% |

Table 5: Recovered values of the parameters $(a_i)_{i=\overline{1,5}}$ and the relative errors (RE%) when both the dimensionless boundary temperatures $\theta(0,t)$ and $\theta(1,t)$ are measured.

| | | $p=0$ | | $p=0.1\%$ | |
|---|---|---|---|---|---|
| | exact | numerical | RE% | numerical | RE% |
| $a_1$ | 5.4 | 5.3991 | 0.02% | 5.3949 | 0.09% |
| $a_2$ | 0.05639 | 0.05627 | 0.21% | 0.05607 | 0.56% |
| $a_3$ | 7.2 | 7.1878 | 0.17% | 7.1671 | 0.46% |
| $a_4$ | 0.05 | 0.04996 | 0.08% | 0.04993 | 0.15% |
| $a_5$ | 11.299 | 11.2998 | $2.3\times10^{-3}$% | 11.3005 | $8.2\times10^{-3}$% |
| $G^{\text{ideal}}$ | | $4.77\times10^{-3}$ | | $8.937\times10^{-2}$ | |
| Value of objective function $G$ | | $3.62\times10^{-3}$ | | $8.584\times10^{-2}$ | |
| Number of iterations | | 83 | | 83 | |
| Computational time | | 53 seconds | | 57 seconds | |
| Reason of halting iteration | | *lsqnonlin* solver exceeded function evaluation limit, 500 | | | |

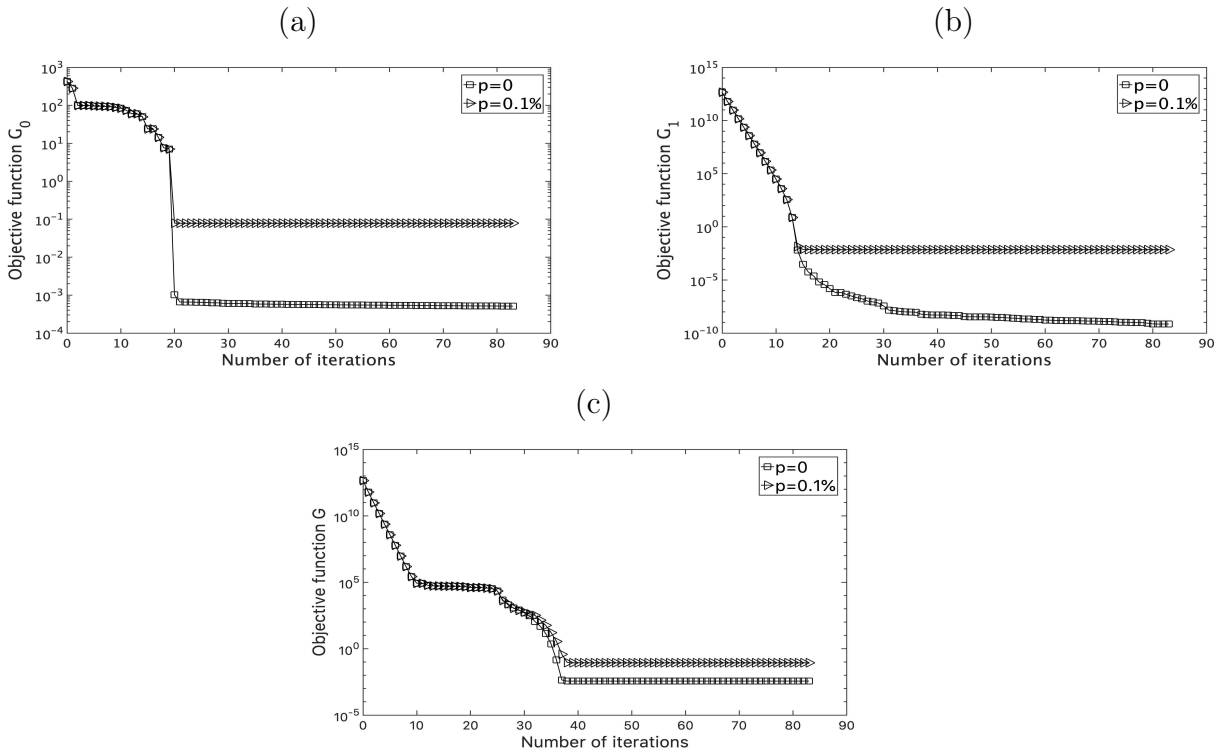


Figure 7: The objective functions $G_0$, $G_1$ and $G$ given by (46), (47) and (45), respectively, as functions of the number of iterations, corresponding to measuring (a) only $\theta(0,t)$, (b) only $\theta(1,t)$ or (c) both $\theta(0,t)$ and $\theta(1,t)$.

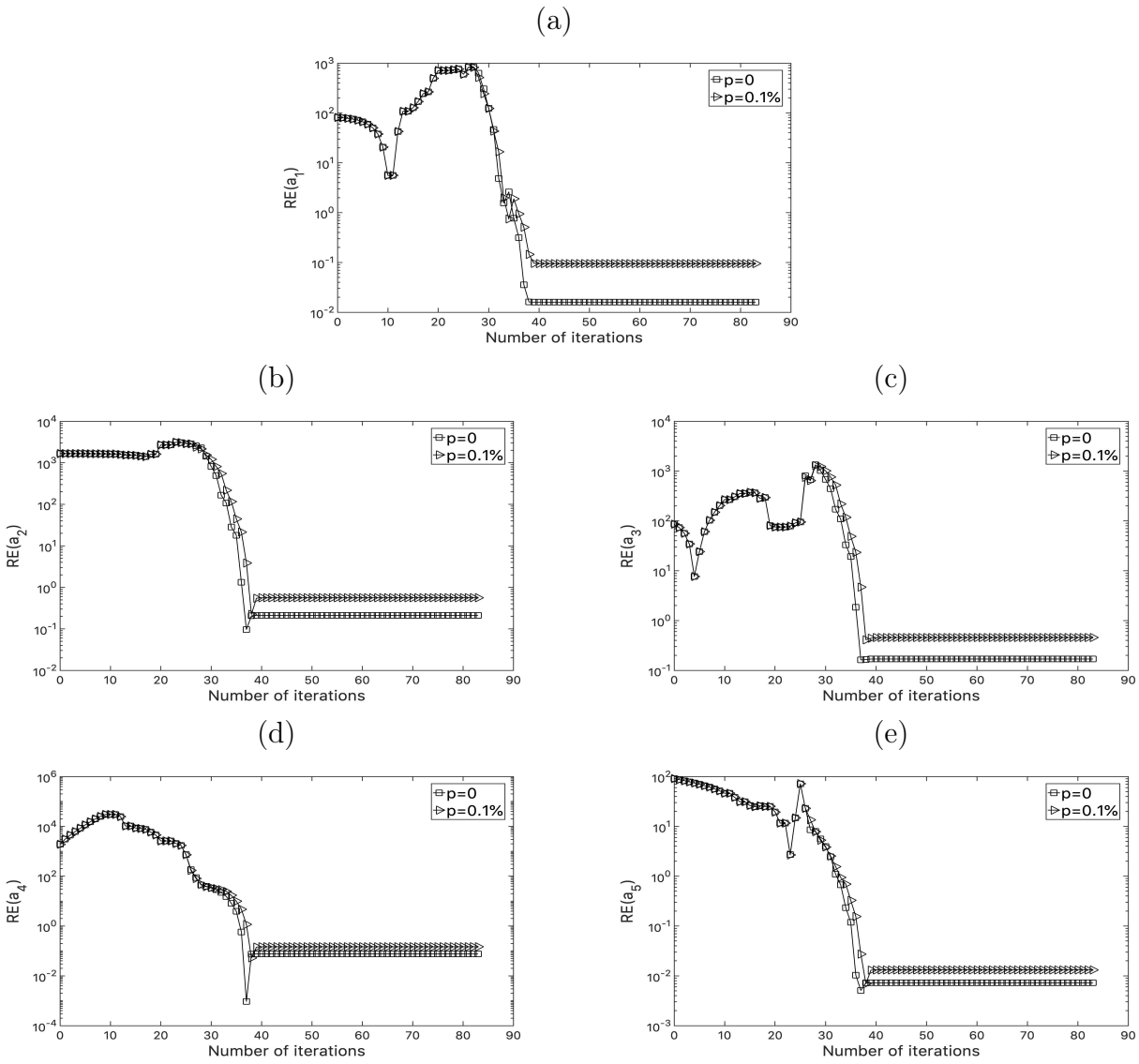


Figure 8: The relative error values (in percentage) defined in (40): (a) RE($a_1$), (b) RE($a_2$), (c) RE($a_3$), (d) RE($a_4$) and (e) RE($a_5$), as functions of the number of iterations, without noise, i.e. $p = 0$, and with $p = 0.1\%$ noise.

Finally, the values of the dimensional constant parameters $w_b$, $R''$, $k$, $\tau$ and $C_\mathrm{t}$ arising in the thermal-wave model given by equations (7), (8) and (11) can be recovered by inverting the system of nonlinear equations defined in (16) to obtain:

$$\tau_\pm = \frac{a_1 t_\mathrm{f} \pm t_\mathrm{f}\sqrt{a_1^2 - 4a_3}}{2a_3}, \quad w_{b_\pm} = \frac{a_2 a_5^2}{t_\mathrm{f}^2}\tau_\pm, \quad R''_\pm = \frac{a_3 a_4 t_\mathrm{f}^2}{(a_2 a_5)^2 L C_b \tau_\pm},$$

$$k_\pm = \frac{\left(a_2 a_5 L\right)^2 C_b}{a_3 t_\mathrm{f}^2}\tau_\pm \quad \text{and} \quad C_\mathrm{t} = \frac{a_2 a_5^2 C_b}{a_3}. \tag{48}$$

From (48), it is interesting to observe that the dimensional inverse problem considered admits mathematically two different solutions (except for the parameter $C_\mathrm{t}$) whose exact and numerical values are outlined in Table 6, along with the relative errors (RE%). A similar situation was also previously encountered in (Flouri et al., 2016), where a dual solution was obtained when solving for a renal two-compartment filtration model using a transformed linear inversion. The solution found using the formulae with the negative sign in (48) is chosen as the desirable solution according to some prior knowledge on the values of the thermo-physical parameters available from the literature (Alkhwaji et al., 2012; Özen et al., 2008).

Table 6: Recovered physical values of $w_b$, $R''$, $k$, $\tau$ and $C_\mathrm{t}$ and the relative errors (RE%).

| (a) Solution found using the positive sign in (48) | | | | | |
|---|---|---|---|---|---|
| | | $p = 0$ | | $p = 0.1\%$ | |
| | exact | numerical | RE% | numerical | RE% |
| $w_{b_+}$ | 0.05 | 0.0502 | 0.48% | 0.0504 | 0.83% |
| $R''_+$ | 0.0016 | $1.592 \times 10^{-3}$ | 0.51% | $1.586 \times 10^{-3}$ | 0.86% |
| $k_+$ | 0.625 | 0.6277 | 0.44% | 0.6295 | 0.72% |
| $\tau_+$ | 25 | 25.172 | 0.69% | 25.346 | 1.38% |
| $C_\mathrm{t}$ | $3.99 \times 10^6$ | $3.988 \times 10^6$ | 0.04% | $3.986 \times 10^6$ | 0.09% |
| (b) Solution found using the negative sign in (48) | | | | | |
| | | $p = 0$ | | $p = 0.1\%$ | |
| | exact | numerical | RE% | numerical | RE% |
| $w_{b_-}$ | 0.04 | 0.0397 | 0.72% | 0.0394 | 1.45% |
| $R''_-$ | 0.002 | $2.014 \times 10^{-3}$ | 0.69% | $2.029 \times 10^{-3}$ | 1.43% |
| $k_-$ | 0.5 | 0.4962 | 0.76% | 0.4922 | 1.56% |
| $\tau_-$ | 20 | 19.897 | 0.52% | 19.818 | 0.91% |
| $C_\mathrm{t}$ | $3.99 \times 10^6$ | $3.988 \times 10^6$ | 0.04% | $3.986 \times 10^6$ | 0.09% |

From the third and fourth columns of Table 6(b), it can be seen that accurate and stable numerical results have been successfully achieved for the simultaneous reconstruction of all the five dimensional constant unknowns of interest, arising in the thermal-wave model given by equations (7), (8) and (11), for noiseless data, i.e. $p = 0$. In addition, the average relative error (ERR%) defined in equation (41) is 0.55% for this recovery. Similarly, from the fifth and sixth columns of Table 6(b), it can be seen that accurate and stable numerical results have been successfully achieved for the simultaneous reconstruction of all the five dimensional

constant unknowns when the percentage of noise is $p = 0.1\%$. A comparison between the fourth and sixth columns of the same table reveals that the presence of measurement error only alters the accuracy of the recovered values of the unknowns slightly, as the average relative error (ERR%) defined in equation (41) is only 1.09% for $p = 0.1\%$ noise compared to 0.55% for $p = 0$.

To sum up, the results of Tables 5 and 6(b), and Figure 8 confirm that accurate and stable numerical reconstruction of all the five thermo-physical dimensional constant parameters, that are: the blood perfusion rate $w_b$, the thermal contact resistance $R''$, the thermal conductivity $k$, the relaxation time $\tau$ and the heat capacity of tissue $C_{\rm t}$, from both exact and noisy (for up to $p = 0.1\%$ noise) dimensionless boundary temperatures at $x \in \{0, 1\}$, has been achieved using the MATLAB optimization toolbox routine *lsqnonlin*. As for a higher percentage of noise such as 1%, it was found that some relative errors (RE%) of the recovered dimensional parameters are of about 10% and thus the results for this level of noise are not presented.

# 7 Conclusions

In this paper, an investigation into the numerical retrieval of five constant thermo-physical parameters arising in a thermal-wave model of bio-heat transfer has been carried out. For the numerical discretization, an unconditionally stable FDM was used as a direct solver. Accurate and stable numerical results for the simultaneous reconstruction of the five constant thermo-physical parameters, that are: the blood perfusion rate $w_b$, the thermal contact resistance $R''$, the thermal conductivity $k$, the relaxation time $\tau$ and the heat capacity of tissue $C_{\rm t}$ arising in the dimensional thermal-wave model of interest has been successfully achieved through a minimization procedure based on the MATLAB optimization toolbox routine *lsqnonlin*, when both the dimensionless boundary temperatures at $x \in \{0, 1\}$ are measured for $p = 0$ and $p = 0.1\%$ noise. It was found that the considered dimensional inverse problem mathematically admits two solutions; one of which may correspond to the true thermo-physical properties of the one-layered, one-dimensional tissue slab considered, as found from the literature (Alkhwaji et al., 2012; Özen et al., 2008).

A possible direction of further work is the determination of the same thermo-physical properties recovered in this paper, but for a multi-layered tissue stratified into epidermis, dermis, subcutaneous and inner tissue (Özen et al., 2008).

# References

[1] Ahmadikia, H., Fazlali, R. and Moradi, A. (2012), "Analytical solution of the parabolic and hyperbolic heat transfer equations with constant and transient heat flux conditions on skin tissue", *International Communications in Heat and Mass Transfer*, Vol. 39 No. 1, pp. 121–130.

[2] Alkhwaji, A., Vick, B. and Diller, T. (2012), "New mathematical model to estimate tissue blood perfusion, thermal contact resistance and core temperature", *Journal of Biomechanical Engineering-Transactions of the ASME*, Vol. 134 No. 081004, 8 pp.

[3] Bazán, F.S.V., Bedin, L. and Borges, L.S. (2017), "Space-dependent perfusion coefficient estimation in a 2D bioheat transfer problem", *Computer Physics Communications*, Vol. 214, pp. 18–30.

[4] Beck, J.V. and Arnold, K.J. (1985), *Parameter Estimation in Engineering and Science*, John Wiley & Sons, New York.

[5] Bertman, B. and Sandiford, D.J. (1970), "Second sound in solid helium", *Scientific American*, Vol. 222 No. 5, pp. 92–101.

[6] Cao, K. and Lesnic, D. (2018), "Reconstruction of the space-dependent perfusion coefficient from final time or time-average temperature measurements", *Journal of Computational and Applied Mathematics*, Vol. 337, pp. 150–165.

[7] Cao, L., Qin, Q.-H. and Zhao, N. (2010), "An RBF–MFS model for analysing thermal behaviour of skin tissues", *International Journal of Heat and Mass Transfer*, Vol. 53 Nos 7/8, pp. 1298–1307.

[8] Cattaneo, M.C. (1958), "Sur une forme de l'équation de la chaleur éliminant le paradoxe d'une propagation instantanée", *Comptes rendus de l'Académie des Sciences*, Vol. 247 No. 4, pp. 431–433.

[9] Chan, C.L. (1992), "Boundary element method analysis for the bioheat transfer equation", *Journal of Biomechanical Engineering-Transactions of the ASME*, Vol. 114 No. 3, pp. 358–365.

[10] Chester, M. (1963), "Second sound in solids", *Physical Review*, Vol. 131 No. 5, pp. 2013–2015.

[11] Coleman, T.F. and Li, Y. (1996), "An interior trust region approach for nonlinear minimization subject to bounds", *SIAM Journal on Optimization*, Vol. 6 No. 2, pp. 418–445.

[12] Dai, W. and Nassar, R. (1999), "A finite difference scheme for solving the heat transport equation at the microscale", *Numerical Methods for Partial Differential Equations*, Vol. 15 No. 6, pp. 697–708.

[13] Firoozan, M.S., Porkhial, S. and Nejad, A.S. (2015), "Effect of tissue and atmosphere's parameters on human eye temperature distribution", *Journal of Thermal Biology*, Vol. 47, pp. 51–58.

[14] Flouri, D., Lesnic, D. and Sourbron, S.P. (2016), "Fitting the two-compartment model in DCE-MRI by linear inversion", *Magnetic Resonance in Medicine*, Vol. 76 No. 3, pp. 998–1006.

[15] Gao, B., Langer, S. and Corry, P.M. (1995), "Application of the time-dependent Green's function and Fourier transforms to the solution of the bioheat equation", *International Journal of Hyperthermia*, Vol. 11 No. 2, pp. 267–285.

[16] Hafid, M. and Lacroix, M. (2017), "Fast inverse prediction of the freezing front in cryosurgery", *Journal of Thermal Biology*, Vol. 69, pp. 13–22.

[17] Hennessy, M.G., Calvo-Schwarzwälder, M. and Myers, T.G. (2019), "Modelling ultra-fast nanoparticle melting with the Maxwell–Cattaneo equation", *Applied Mathematical Modelling*, Vol. 69, pp. 201–222.

[18] Hsu, P.-T. (2006), "Estimating the boundary condition in a 3D inverse hyperbolic heat conduction problem", *Applied Mathematics and Computation*, Vol. 177 No. 2, pp. 453–464.

[19] Huntul, M., Lesnic, D. and Johansson, B.T. (2018), "Determination of an additive time- and space-dependent coefficient in the heat equation", *International Journal of Numerical Methods for Heat & Fluid Flow*, Vol. 28 No. 6, pp. 1352–1373.

[20] Kengne, E. and Lakhssassi, A. (2015), "Bioheat transfer problem for one-dimensional spherical biological tissues", *Mathematical Biosciences*, Vol. 269, pp. 1–9.

[21] Lee, H.-L., Lai, T.-H, Chen, W.-L. and Yang, Y.-C. (2013), "An inverse hyperbolic heat conduction problem in estimating surface heat flux of a living skin tissue", *Applied Mathematical Modelling*, Vol. 37 No. 5, pp. 2630–2643.

[22] Liu, J., Chen, X. and Xu, L.X. (1999), "New thermal wave aspects on burn evaluation of skin subjected to instantaneous heating", *IEEE Transactions on Biomedical Engineering*, Vol. 46 No. 4, pp. 420–428.

[23] Liu, J., Ren, Z. and Wang, C. (1995), "Interpretation of living tissue's temperature oscillations by thermal wave theory", *Chinese Science Bulletin*, Vol. 40 No. 17, pp. 1493–1495.

[24] Liu, J. and Xu, L.X. (2000), "Boundary information based diagnostics on the thermal states of biological bodies", *International Journal of Heat and Mass Transfer*, Vol. 43 No. 16, pp. 2827–2839.

[25] Mathworks (2012), "Documentation optimization toolbox-least squares (model fitting) algorithms", available at: www.mathworks.com/help/toolbox/optim/ug/brnoybu.html.

[26] Mitra, K., Kumar, S., Vedavarz, A. and Moallemi, M.K. (1995), "Experimental evidence of hyperbolic heat conduction in processed meat", *Journal of Heat Transfer-Transactions of the ASME*, Vol. 117 No. 3, pp. 568–573.

[27] Mochnacki, B. and Tuzikiewicz,W. (2016), "Cattabeo-Vernotte bioheat transfer equation. Stability conditions of numerical algorithm based on the explicit scheme of the finite difference method", *Journal of Applied Mathematics and Computational Mechanics*, Vol. 15 No. 4, pp. 137–144.

[28] Narasimhan, A. and Sadasivam, S. (2013), "Non-Fourier bio heat transfer modelling of thermal damage during retinal laser irradiation", *International Journal of Heat and Mass Transfer*, Vol. 60, pp. 591–597.

[29] Nóbrega, S. and Coelho, P.J. (2017), "A parametric study of thermal therapy of skin tissue", *Journal of Thermal Biology*, Vol. 63, pp. 92–103.

[30] Özen, Ş., Helhel, S. and Çerezci, O. (2008), "Heat analysis of biological tissue exposed to microwave by using thermal wave model of bio-heat transfer (TWMBT)", *Burns*, Vol. 34 No. 1, pp. 45–49.

[31] Özişik, M.N. and Orlande, H.R.B. (2000), *Inverse Heat Transfer: Fundamentals and Applications*, Taylor & Francis, New York.

[32] Pennes, H.H. (1948), "Analysis of tissue and arterial blood temperatures in the resting human forearm", *Journal of Applied Physiology*, Vol. 1 No. 2, pp. 93–122.

[33] Peshkov, V.P. (1960), "Second sound in helium II", *Soviet Physics JETP*, Vol. 11 No. 3, pp. 580–584.

[34] Vernotte, P. (1958), "Les paradoxes de la théorie continue de léquation de la chaleur", *Comptes rendus de l'Académie des Sciences*, Vol. 246 No. 22, pp. 3154–3155.

[35] Yang, C.-y. (2014), "Boundary prediction of bio-heat conduction in a two-dimensional multilayer tissue", *International Journal of Heat and Mass Transfer*, Vol. 78, pp. 232–239.

[36] Yu, Y.J. (2018), "Analytical solutions to hyperbolic heat conductive models using Green's function method", *Journal of Thermal Science and Technology*, Vol. 13 No. 1, pages JTST0012.

[37] Zhang, X., Chapal Hossain, S.M., Zhao, G., Qiu, B. and He, X. (2017), "Two-phase heat transfer model for multiprobe cryosurgery", *Applied Thermal Engineering*, Vol. 113, pp. 47–57.

[38] Zhang, A., Luo, X., Chen, C., He, L. and Xu, L.X. (2006), "Numerical simulation of tissue freezing by liquid nitrogen based cryoprobe", *CryoLetters*, Vol. 27 No. 4, pp. 243–252.

[39] Zhao, J.J., Zhang, J., Kang, N. and Yang, F. (2005), "A two level finite difference scheme for one dimensional Pennes' bioheat equation", *Applied Mathematics and Computation*, Vol. 171 No. 1, pp. 320–331.

[40] Zhukovsky, K.V. and Srivastava, H.M. (2017), "Analytical solutions for heat diffusion beyond Fourier law", *Applied Mathematics and Computation*, Vol. 293, pp. 423–437.